contribution $[R]_{conf}$ is calculated to be −0.15 (corresponding to an equilibrium distribution of 50.43% **2**eq: 49.57% **2**ax). Our studies indicate that in situations where a molecule can assume conformations which possess large and oppositely signed rotational strengths, the presence of a conformational isotope effect can complicate the interpretation of the chiroptical data and lead to ambiguous conclusions with respect to the determination of absolute configurations.

## Experimental Section

Circular dichroism spectra were recorded on a JASCO J-40 instrument using a previously described[18] cell for the low-temperature measurements. Absorption spectra were measured with a Hewlett-Packard HP 8450A UV–vis spectrophotometer. Optical rotations were determined on a Rudolf Autopol III polarimeter in a thermostated 10-cm cell using chloroform as solvent. Infrared (IR) spectra were recorded as neat liquid films between NaCl plates on a Perkin-Elmer 700A spectrometer. $^1$H NMR spectra were obtained on a Varian T-60 spectrometer and given as $\delta$ values using deuteriochloroform as solvent and tetramethylsilane as internal standard. Mass spectra (MS) were obtained on a Varian MAT-44 spectrometer. High resolution mass spectra were determined by Ms. A. Wegmann on a Varian MAT-711 spectrometer; both instruments operated at 70 eV with a direct inlet system.

**(1*S*,2*S*)-Epoxycyclopentane-1-methanol (5).** Epoxidation of cyclopentene-1-methanol (**4**)[7] (9 g, 0.1 mol), using the modified procedure of Sharpless et al.,[6] gave after distillation 4 g (38% yield) of **5**: bp 52–53 °C (0.05 mm); $[\alpha]^{20}_D$ −23.92° (0.054); IR 3175 cm$^{-1}$; $^1$H NMR: 1.5–1.8 (m, 6 H), 3.46 (s, 1 H), 3.83 (d, 1 H, $J$ = 14 Hz), 3.86 (d, 1 H, $J$ = 14 Hz); MS $m/z$ 114 (12, M$^+$), 97 (23), 96 (20), 86 (28), 83 (56), 71 (23), 70 (95), 67 (30), 57 (77), 55 (100); mol wt (calcd for $C_6H_{10}O_2$) 114.06807, found 114.0671.

**(1*R*,2*R*)-[2-$^2$H$_1$]-1-Hydroxycyclopentane-1-methanol (6).** Reduction of the epoxide **5** (2 g, 0.017 mol) with 2 g of $LiAlD_4$ in refluxing ether (12 h) gave 1.09 g (50% yield) of the diol **6**: IR 3175 cm$^{-1}$; $^1$H NMR 1.63 (bs, 5 H), 3.36 (bs, 2 H), 3.56 (q, 2 H, $J$ = 6 Hz); MS $m/z$ 117 (28, M$^+$), 86 (100), 70 (53), 68 (50), 58 (30), 57 (30), 42 (48), 41 (40).

**(1*R*,2*R*)-1-Hydroxy-2-methylcyclopentane-1-methanol (7).** The epoxy alcohol **5** (1.16 g, 0.01 mol) was added to a solution of $(CH_3)_2CuLi$ (prepared from 7 g of cuprous bromide and 70 mL of 1.5 M methyllithium) in 150 mL of anhydrous ether. The reaction mixture was stirred at room temperature for 12 h. After workup and chromatography on silica gel using ether as eluting solvent, 0.5 g of **7** was obtained (37% yield); $[\alpha]^{20}_D$ 26.6° (0.0225); IR 3175 cm$^{-1}$; $^1$H NMR 0.9 (d, 3 H, $J$ = 8 Hz), 1.4–2.3 (m, 7 H), 3.47 (d, 1 H, $J$ = 14 Hz), 3.60 (d, 1 H, $J$ = 14 Hz); MS $m/z$ 130 (1, M$^+$), 99 (60, M − $CH_2OH$), 87 (15), 81 (40), 55 (40), 43 (100), 41 (40).

**(*R*)-[2-$^2$H$_1$]Cyclopentanone (2).** The diol **6** (234 mg, 2 mmol) in 0.5 mL of wet ether was added to a solution of 470 mg (2 mmol) of periodic acid in 10 mL of ether and the mixture stirred for 30 min at room temperature, then cooled to −20 °C and filtered over a small amount of silica gel. Evaporation of the ether followed by bulb to bulb distillation at 140 °C gave **2**: MS $m/z$ 85 (55, M$^+$), 56 (50), 55 (82), 45 (42), 43 (40), 31 (100); isotopic purity 98%. Since the samples contained small amounts of ether, the concentrations for the CD measurements were determined from the absorption spectrum ($\epsilon_{278}$ 17.7 methanol, $\epsilon_{300}$ 17.2 isooctane): CD $[\theta]_{312}$, −139, $[\theta]_{285}$ 42 (isooctane); $[\theta]_{304}$ −84, $[\theta]_{272}$ 42 (methanol). Somewhat smaller values were reported by Dauphin et al.[5] for material prepared by enzymatic means: $[\theta]_{299}$ −55, $[\theta]_{274}$ 22 (ethanol).

**(*R*)-2-Methylcyclopentanone (3).** The periodide oxidation of **7** was performed as outlined for **2**. The concentrations for the CD measurements were determined from the absorption spectra ($\epsilon_{298}$ 17.9 isooctane, $\epsilon_{287}$ 19.3 methanol: CD $[\theta]_{297}$ −6040 (methanol), $[\theta]_{310}$ −6650 (isooctane). Other spectral properties (IR, $^1$H, NMR) were identical with those of an authentic sample (Columbia Organic Chemicals Co., Inc., Columbia, Ohio) of racemic 2-methylcyclopentanone.

**Acknowledgment.** This work was supported by a grant (No. CHE 78-27413) from the National Science Foundation. We are grateful to Professor A. Kergomard (University of Clermont, Aubiere, France) for providing us with the results of his work prior to publication (ref 5). We are especially grateful to Professor K. B. Sharpless (Chemistry Department, Massachusetts Institute of Technology, Cambridge) for experimental details relating to the chiral epoxidation steps.

(18) Barth, G.; Dawson, J. H.; Dollinger, P. M.; Linder, R. E.; Bunnenberg, E.; Djerassi, C. *Anal. Biochem.* **1975**, *65*, 100–108.

# Polymer Films on Electrodes. 5. Electrochemistry and Chemiluminescence at Nafion-Coated Electrodes

**Israel Rubinstein and Allen J. Bard***

*Contribution from the Department of Chemistry, The University of Texas, Austin, Texas 78712.*
*Received December 4, 1980*

**Abstract:** The electrochemical behavior of 10–15-$\mu$m thick films of the cation-exchange polymer Nafion on substrates of pyrolytic graphite, glassy carbon or platinum-containing $Ru(bpy)_3^{2+}$ (bpy = 2,2′-bipyridine) (or other cations) is described. The reaction of electrogenerated $Ru(bpy)_3^{3+}$ with oxalate dissolved in the solution leads to production of $Ru(bpy)_3^{2+*}$ and light emission. A model for the reaction scheme is proposed and digital simulation of the current–potential and current– and light emission–time curves allowed estimation of the rate constants for various processes and apparent diffusion coefficients of the species in the polymer film. The results provide information about the mechanism of excited-state production, with evidence for penetration of the polymer film by oxalate and also possible quenching of $Ru(bpy)_3^{2+*}$ by $Ru(bpy)_3^{3+}$.

In a recent communication[1] we described a new type of polymer-coated modified electrode, which consisted of pyrolytic graphite (PG) coated with a layer of Nafion ion-exchange polymer,[2] in which a large amount of $Ru(bpy)_3^{2+}$ (where bpy = 2,2′-bipyridine) was incorporated by electrostatic binding.[3] This modified electrode was shown to exhibit large oxidation–reduction waves for the attached $Ru(bpy)_3^{2+}$, to be exceptionally stable in aqueous solution, and to catalyze some oxidation reactions.

In aqueous solutions containing oxalate ions at pH ~6, switching the potential of this electrode to the $Ru(bpy)_3^{2+}$ oxidation

(1) Rubinstein, I.; Bard, A. J. *J. Am. Chem. Soc.* **1980**, *102*, 6641.
(2) Nafion is a perfluorinated sulfonated polymer produced by the E.I. duPont de Nemours and Co. See: Grot, W. *Chem.-Ing.-Tech.* **1978**, *50*, 299.
(3) Oyama, N.; Anson, F. C. *J. Electrochem. Soc.* **1980**, *127*, 247; Oyama, N.; Shimomura, T.; Shigehara, K.; Anson, F. C. *J. Electroanal. Chem.* **1980**, *112*, 271.

0002-7863/81/1503-5007$01.25/0 

potential resulted in the production of intense orange light emission, identified as the luminescence of the bound $Ru(bpy)_3^{2+*}$ species. We suggested that analysis of the nature of the observed electrogenerated chemiluminescence (ecl) emission, and its dependence on electrode potential and time, along with more conventional electrochemical measurements, could be beneficial in evaluating the mechanism of charge and mass transfer and the nature of catalysis within the polymer layers on electrodes.

Much effort has been directed in recent years to the preparation and investigation of polymer-coated modified electrodes.[1,3-29] Special attention has been given to the possible catalytic properties of such electrodes,[1,6,17-22] the nature of the charge and mass transfer through the polymer layer,[6,10,14-16,19,25] and theoretical treatment of the parameters determining the rate of the electrochemical reaction[14,15,28] and the catalytic process on polymer-coated electrodes.[26-29] The role of the various factors, e.g., the rate of electron transfer at the electrode–polymer interface, the rate of electron transfer through the polymer, counterion diffusion, and substrate penetration into the polymer, on the rate of reaction is not always clear and distinguishable and probably varies for different polymers.

In this work we describe further investigation of the nature of Nafion-coated electrodes. The combined electrochemical and ecl data are used to evaluate a model for the different processes occurring at the modified electrode during oxidation of the attached $Ru(bpy)_3^{2+}$ species in the absence as well as in the presence of oxalate ions in solution. The validity of the model is tested by digital simulation techniques.

## Experimental Section

Electrochemical measurements were performed as previously described.[30] Ecl intensities were measured with a Hamamatsu R928 photomultiplier tube. Glassy carbon (GC) was obtained from Atomergic Chemicals Co.. Pyrolytic graphite was supplied by Union Carbide Corp.; the basal plane was used as the active surface. Electrodes were prepared by sealing the carbon material in shrinkable Teflon[5] and yielded working electrode geometric areas of ~0.2 $cm^2$. The electrodes were dip-coated with Nafion polymer following the procedure described elsewhere.[1] An ethanolic solution of ~2% low molecular weight Nafion (equiv wt ~ 970), produced by E. I. duPont de Nemours and Co. was employed. The thickness of the polymer layers (wet) was measured with a Dektak profilometer (manufactured by Sloan Technology Corp.) and is about twice the dry thickness calculated from the weight of the film and the dry density of Nafion (2 $g/cm^3$). Sodium oxalate (Allied Chemicals), sodium sulfate (Fischer Scientific Co.), $Ru(bpy)_3Cl_2$ (G. F. Smith Chemical Co.), and methyl viologen ($MV^{2+}$, 4,4′-dimethylpyridinum dichloride) (Sigma Chemical Co.) were used without further purification. The $Fe(tpd)_2^{2+}$ solution (where tpd = 2,2′,2″-terpyridine) was prepared by dissolving $FeSO_4$ and an excess of the ligand in 0.5 M $H_2SO_4$. $Ru(bpy)_3(ClO_4)_2$ was prepared as described elsewhere.[31] All solutions were prepared with triply distilled water.

In all current–potential curves, anodic current is drawn in an upward direction.

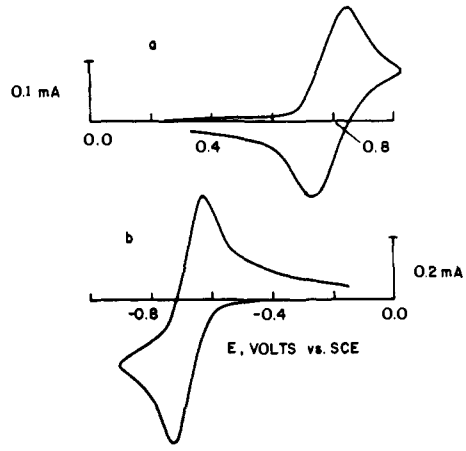


**Figure 1.** Current–potential curves of Nafion-coated electrodes: (a) PG/Nafion, $Fe(tpd)_2^{2+}$ in 0.2 M $Na_2SO_4$ adjusted to pH 2 with $H_2SO_4$; (b) Pt/Nafion, $MV^{2+}$ in 0.2 M $Na_2SO_4$ (tpd = terpyridine, $MV^{2+}$ = methyl viologen; scan rate = 100 mV/s).

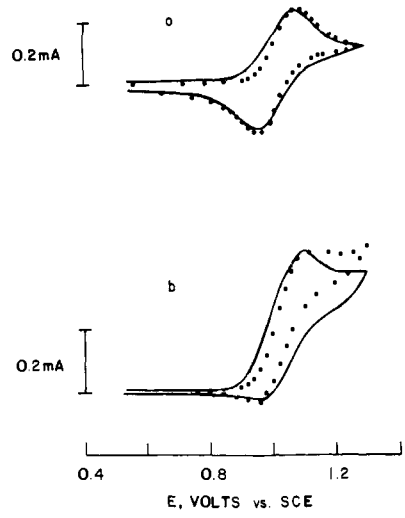


**Figure 2.** Current–potential curves for PG/Nafion, $Ru(bpy)_3^{2+}$: (a) in 0.2 M $NaClO_4$; (b) as in a, with 50 mM $Na_2C_2O_4$ in the solution (scan rate = 100 mV/s): —, experimental; ●, simulated (for details, see text).

## Results and Discussion

**Properties of Nafion-Coated Electrodes.** Nafion-coated electrodes prepared by dip-coating[1] have a rather thick coating, usually 10–15 μm (wet). The use of different electrode substrate materials, e.g., PG, GC, or Pt, yields electrodes showing virtually the same behavior. Large amounts of electroactive cationic species, of the order of several hundred millimolar (which corresponds to ~3 × $10^{-7}$ mol/$cm^2$ of electrode surface and is 1 order-of-magnitude lower than estimated previously[1]), can be incorporated and strongly held in the polymer layer by dipping the Nafion-coated electrode in an acidic solution of the specific cation. Figures 1 and 2a are current–potential curves for three different electroactive species incorporated into the electrode in background solutions. Although the Nafion-coating is transparent, electrodes containing Ru-

(4) Oyama, N.; Anson, F. C. *J. Electrochem. Soc.* **1980**, *127*, 640.
(5) Oyama, N.; Anson, F. C. *J. Am. Chem. Soc.* **1979**, *101*, 3450.
(6) Oyama, N.; Anson, F. C. *Anal. Chem.* **1980**, *52*, 1192.
(7) Snell, K. D.; Keenan, A. G. *Chem. Soc. Rev.* **1979**, *8*, 259.
(8) Bocarsly, A. B.; Walton, E. G.; Wrighton, M. S. *J. Am. Chem. Soc.* **1980**, *102*, 3390.
(9) Daum, P.; Murray, R. W. *J. Electroanal. Chem.* **1979**, *103*, 289.
(10) Nowak, R. J.; Schultz, F. A.; Umana, M.; Lam, R.; Murray, R. W. *Anal. Chem.* **1980**, *52*, 315.
(11) Merz, A.; Bard, A. J. *J. Am. Chem. Soc.* **1978**, *100*, 3222.
(12) Itaya, K.; Bard, A. J. *Anal. Chem.* **1978**, *50*, 1487.
(13) Peerce, P. J.; Bard, A. J. *J. Electroanal. Chem.* **1980**, *108*, 121.
(14) Peerce, P. J.; Bard, A. J. *J. Electroanal. Chem.* **1980**, *112*, 97.
(15) Peerce, P. J.; Bard, A. J. *J. Electroanal. Chem.* **1980**, *114*, 89.
(16) Kaufman, F. B.; Engler, E. M. *J. Am. Chem. Soc.* **1979**, *101*, 547.
(17) Van De Mark, M. R.; Miller, L. L. *J. Am. Chem. Soc.* **1978**, *100*, 3223.
(18) Kerr, J. B.; Miller, L. L. *J. Electroanal. Chem.* **1979**, *101*, 263.
(19) Kerr, J. B.; Miller, L. L.; Van De Mark, M. R. *J. Am. Chem. Soc.* **1980**, *102*, 3383.
(20) Degrand, C.; Miller, L. L. *J. Am. Chem. Soc.* **1980**, *102*, 5728.
(21) Landrum, H. L.; Salmon, R. T.; Hawkridge, F. M. *J. Am. Chem. Soc.* **1977**, *99*, 3154.
(22) Dautartas, M. F.; Evans, J. F. *J. Electroanal. Chem.* **1980**, *109*, 301.
(23) Samuels, G. J.; Meyer, T. J. *J. Am. Chem. Soc.*, in press.
(24) Diaz, A. F.; Lee, W.-Y.; Logan, A. *J. Electroanal. Chem.* **1980**, *108*, 377.
(25) Doblhofer, K. *Electrochim. Acta* **1980**, *25*, 871.
(26) Andrieux, C. P.; Saveant, J. M. *J. Electroanal. Chem.* **1978**, *93*, 163; **1980**, *111*, 377.
(27) Andrieux, C. P.; Dumas-Bouchiat, J. M.; Saveant, J. M. *J. Electroanal. Chem.*, in press.
(28) Laviron, E. *J. Electroanal. Chem.* **1980**, *112*, 1.
(29) Laviron, E.; Roullier, L.; Degrand, C. *J. Electroanal. Chem.* **1980**, *112*, 11.
(30) Rubinstein, I.; Bard, A. J. *J. Am. Chem. Soc.* **1981**, *103*, 512 and references therein.
(31) Tokel-Takvoryan, N. E.; Hemingway, R. E.; Bard, A. J. *J. Am. Chem. Soc.* **1973**, *95*, 6582.

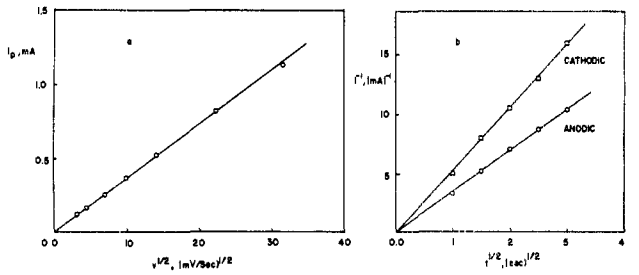


**Figure 3.** (a) Scan rate dependence of the anodic peak current for PG/Nafion, $Ru(bpy)_3^{2+}$ in 0.2 M $Na_2SO_4$. (b) $i$–$t^{1/2}$ (Cottrell) plots for steps to the diffusion-limited region for PG/Nafion, $Ru(bpy)_3^{2+}$ in 0.2 M $Na_2SO_4$ or 0.2 M $NaClO_4$.

$(bpy)_3^{2+}$ or $Fe(tpd)_2^{2+}$ show a deep orange or purple color, respectively, a visual indication of the large amount of material incorporated in the polymer. Pt/Nafion, $MV^{2+}$ electrodes are colorless, but become deep purple when the $MV^{2+}$ is reduced to the purple form, $MV^{+\cdot}$. Oxidation of $MV^{+\cdot}$ back to $MV^{2+}$ restores the colorless surface. All these electrodes are extremely stable in aqueous solutions, and repetitive cycling of the potential for prolonged periods of time (e.g., 7 h) only slightly reduces the peak currents.[1] Although Nafion is a cation-exchange material, coated electrodes also are capable of extracting uncharged molecules, e.g., ferrocene (Fc), from aqueous solution,[32] as evidenced by the growth of the $Fc/Fc^+$ redox waves upon repetitive cycling of the potential of a Nafion-coated electrode dipped in a ferrocene-saturated aqueous solution. In this case, however, the electroactive molecules are extracted into the less polar part of the polymer structure. The fact that Nafion provides a low dielectric-constant environment has been recently demonstrated[33-35] for Nafion 120 membranes, which were shown to be much more selective for large organic cations than for small inorganic cations like $Na^+$ or $K^+$.

The luminescence spectrum of the bound $Ru(bpy)_3^{2+}$ and its Raman spectrum[36] were identical with those of the species in aqueous solution. This is in agreement with the proposed cluster-type model for the structure of Nafion polymer,[33,34] in which the $Ru(bpy)_3^{2+}$ ions are located in an environment very similar to bulk water. Note, however, that Lee and Meisel[34] found a small blue shift in the luminescence spectrum of $Ru(bpy)_3^{2+}$ bound to Nafion membranes made of higher equivalent weight material. The difference between the results with Nafion-coated electrodes and Nafion membranes is very likely the result of the difference in structure between the membranes and the low equivalent weight polymer, with the latter being more porous with larger clusters and a higher water content. Other properties such as the penetration of small anions are also different for the two types of Nafion, probably for the same reasons, as discussed below.

**Electrochemical Measurements with Nafion-Coated Electrodes.** A typical current-potential curve for a PG/Nafion, $Ru(bpy)_3^{2+}$ electrode is shown in Figure 2a. The shape of the waves is very different from that expected for a surface-confined species,[37] (i.e., symmetrical narrow peaks and anodic and cathodic peak separation, $\Delta E_p$, near zero). Instead, the waves are more diffusion-like, with broad peaks, a nonzero $\Delta E_p$, and a diffusional tail. The $\Delta E_p$ for these electrodes was typically 120–170 mV (at a scan rate, $v$, of 100 mV/s, with iR compensation) which is significantly larger than the near nernstian value of 59 mV found for dissolved $Ru(bpy)_3^{2+}$ oxidation in solution. A large $\Delta E_p$ value usually indicates slow heterogeneous electron transfer. As shown below for the digital simulation results, an apparent value of ca. $10^{-5}$ cm/s has to be assumed for the overall heterogeneous rate constant to account for the experimental $\Delta E_p$ at a scan rate of 100 mV/s

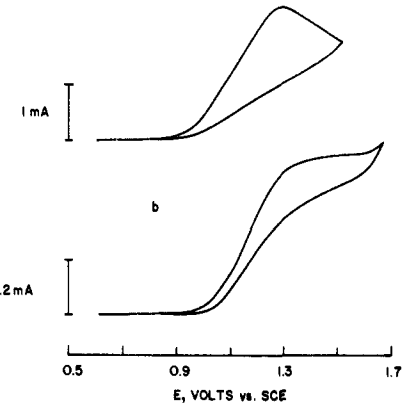


**Figure 4.** Current–potential curves in 0.2 M $Na_2SO_4$ + 50 mM $Na_2C_2O_4$: (a) bare PG electrode; (b) PG/Nafion electrode, scan rate = 100 mV/s.

(Figure 2a). Since the heterogeneous electron-transfer rate for dissolved $Ru(bpy)_3^{2+}$ is quite high, this value for the polymer is surprisingly low. It is possible that other factors, i.e., changes in the structure of the polymer layer upon oxidation and rereduction, which are equivalent to a fast following reaction, contribute to the large $\Delta E_p$ and therefore to the low apparent heterogeneous rate constant.[15] Details of this behavior are currently under investigation.[38]

As shown in Figure 3a, the peak current is proportional to $v^{1/2}$ over the range 0.01–1 V/s. Similar diffusion control in surface layers has been reported in some cases for electroactive polymers[9,10] and is indeed expected for the thick, low-resistant Nafion layers. It may arise from either a real mass-transport limitation within the film (i.e., diffusion of the electroactive species or counterions) or a diffusion-like electron hopping between neighboring electroactive groups bound to the polymer.[16,25,26,28] Counterion diffusion is not likely to be the important factor in this case, since the use of different counterions ($SO_4^{2-}$ and $ClO_4^-$, with different charge and diffusion coefficients)[39] produces indistinguishable results, as illustrated in Figure 3b. Although the present results do not allow one to distinguish between actual $Ru(bpy)_3^{3+/2+}$ diffusion in the film and electron hopping between bound Ru species,[26,28] we will refer to the apparent diffusion coefficients of $Ru(bpy)_3^{2+}$ and $Ru(bpy)_3^{3+}$, $D_2$ and $D_3$, respectively. These diffusion coefficients in the polymer layer were measured by applying potential steps to potentials in the diffusion-controlled region,[40] either oxidizing $Ru(bpy)_3^{2+}$ or reducing $Ru(bpy)_3^{3+}$ in a totally oxidized layer. Figure 3b shows that the current varies at $t^{-1/2}$, as expected for a system following the Cottrell equation.[40] For an average concentration of 0.5 M $Ru(bpy)_3^{2+}$ in the polymer, one calculates $D_2 = 2.7 \times 10^{-9}$ cm$^2$/s and $D_3 = 1.2 \times 10^{-9}$ cm$^2$/s. Note that (a) the diffusion coefficients are rather small, but reasonable, for large positively charged ions in Nafion and (b) these values should only be considered as order-of-magnitude values, since in these thick coatings the concentration of electroactive species changes by as much as a factor of 5 for different coatings. The ratio of $D_2/D_3$, ~2, was, however, reproducible. The difference between the *apparent* diffusion coefficients of the 2+ and 3+ species appears to be the result of a decrease in the fraction of the attached Ru species which is electroactive, upon oxidation of the layer, (i.e., a difference in concentration). This is evident from recent results on thin (<1 μm) Nafion layers,[38] where the apparent diffusion coefficients of both 2+ and 3+ species are identical and in which essentially all of the incorporated ions are available for oxidation or reduction.

A current–potential curve for a PG/Nafion, $Ru(bpy)_3^{2+}$ electrode in the same solution as in Figure 2a, with addition of

(32) Rubinstein, I.; White, H. S.; Bard, A. J., unpublished results.
(33) Gierke, T., paper presented at the Electrochemical Society Meeting, Atlanta, GA, Oct 1977.
(34) Lee, P. C.; Meisel, D. *J. Am. Chem. Soc.* **1980**, *102*, 5477.
(35) Martin, C. R.; Freiser, H. *Anal. Chem.* **1981**, *53*, 902.
(36) Rubinstein, I.; Kress, N.; Woodruff, W. H.; Bard, A. J., unpublished results.
(37) Laviron, E. *J. Electroanal. Chem.* **1972**, *39*, 1; **1974**, *52*, 395.
(38) Martin, C. R.; Rubinstein, I.; Bard, A. J., to be submitted for publication.
(39) Robinson, R. A.; Stokes, R. H. "Electrolytic Solutions"; Butterworth: London, 1955; p 454.
(40) Bard, A. J.; Faulkner, L. R. "Electrochemical Methods"; Wiley: New York, 1980; p 143.

50 mM sodium oxalate, is shown in Figure 2b. Note the greatly enhanced oxidation current and decreased reduction current compared to Figure 2a, illustrating the catalytic oxidation of oxalate via the mediating $Ru(bpy)_3^{3+/2+}$ couple.[30] For completion of the picture, Figure 4 presents current–potential curves for the oxidation of oxalate ions on a bare PG (curve a) and a PG/Nafion (curve b) electrode. A comparison of the three curves in Figures 4 and 2b leads to the following conclusions. (a) Although the peak current for oxalate on Nafion-coated PG is roughly 5 times smaller than that on the bare electrode, oxalate ions still easily penetrate the film to reach the electrode surface. This is in contrast with known properties of Nafion membranes which effectively block anion penetration; this is probably attributable to the more open structure of the low molecular weight polymers, as discussed above. A similar effect was also reported by Oyama and Anson[6] for the diffusion of $Fe^{2+}$ ions through protonated polyvinylpyridine anion-exchange polymer layers on PG and is quite a common phenomenon for diffusion of coions in ion-exchange polymers with a high water content.[41] (b) Although oxalate oxidation of PG/Nafion occurs at potentials more positive than those on the rising portion of the $Ru(bpy)_3^{2+}$ oxidation (and thus $Ru(bpy)_3^{3+}$ mediates the catalytic oxidation of oxalate), some direct oxalate oxidation at the electrode has to be considered in the vicinity of the $Ru(bpy)_3^{3+/2+}$ peak. (c) Because of the very small apparent diffusion coefficient of the Ru species in the polymer, it would take a period of time longer than the duration of the experiment for the charge injected at the substrate/polymer solution interface to traverse the layer to the polymer/solution interface. Thus, the efficient catalytic oxidation of oxalate can be attributed to the fast diffusion of oxalate ions within the polymer layer, in addition to very large concentration of the attached $Ru(bpy)_3^{2+}$.

**Electrogenerated Chemiluminescence.** As previously reported,[1] stepping the potential of a PG/Nafion, $Ru(bpy)_3^{2+}$ electrode (or similarly modified Pt or GC electrodes) to the potential where $Ru(bpy)_3^{2+}$ is oxidized in an aqueous solution at a pH of 4–8 containing oxalate ions produces an intense orange luminescence characteristic of $Ru(bpy)_3^{2+*}$. This results from the sequence of reactions[30] shown in Scheme I followed by (5).

**Scheme I**

$$Ru(bpy)_3^{2+} \rightarrow Ru(bpy)_3^{3+} + e^- \quad (1)$$

$$Ru(bpy)_3^{3+} + C_2O_4^{2-} \xrightarrow{k_1} Ru(bpy)_3^{2+} + C_2O_4^{-}\cdot \quad (2)$$

$$C_2O_4^{-}\cdot \rightarrow CO_2 + CO_2^{-}\cdot \quad (3)$$

$$CO_2^{-}\cdot + Ru(bpy)_3^{3+} \rightarrow CO_2 + Ru(bpy)_3^{2+*} \quad (4a)$$

$$CO_2^{-}\cdot + Ru(bpy)_3^{3+} \xrightarrow{k_3} CO_2 + Ru(bpy)_3^{2+} \quad (4b)$$

$$Ru(bpy)_3^{2+*} \rightarrow Ru(bpy)_3^{2+} + h\nu \quad (5a)$$

$$Ru(bpy)_3^{2+*} \rightarrow Ru(bpy)_3^{2+} \quad (5b)$$

or

$$CO_2^{-}\cdot + Ru(bpy)_3^{2+} \xrightarrow{k_2} CO_2 + Ru(bpy)_3^{+} \quad (6)$$

$$Ru(bpy)_3^{+} + Ru(bpy)_3^{3+} \rightarrow Ru(bpy)_3^{2+*} + Ru(bpy)_3^{2+} \quad (7)$$

An experimental ecl intensity–potential curve for a PG/Nafion, $Ru(bpy)_3^{2+}$ electrode in a solution containing 50 mM oxalate ion during a potential sweep is given in Figure 5a. Note that on the reverse scan the light intensity does not decrease, as the current leading to production of $Ru(bpy)_3^{3+}$ decreases, but rather features an unexpected double-maximum structure. These maxima will be denoted as the first and second reverse peaks, in order of decreasing positive potential. If the oxalate concentration is doubled, a relative decrease in the height of the second reverse peak is observed (Figure 5b). The effect of increasing the scan rate on the ecl intensity, as shown in Figure 5c, is to increase the intensity of the second reverse peak and increase the separation between the forward ecl peak and the second reverse peak. Even

(41) Meares, P. In "Diffusion in Polymers"; Crank, J., Park, G. S., Eds.; Academic Press: London, 1968.

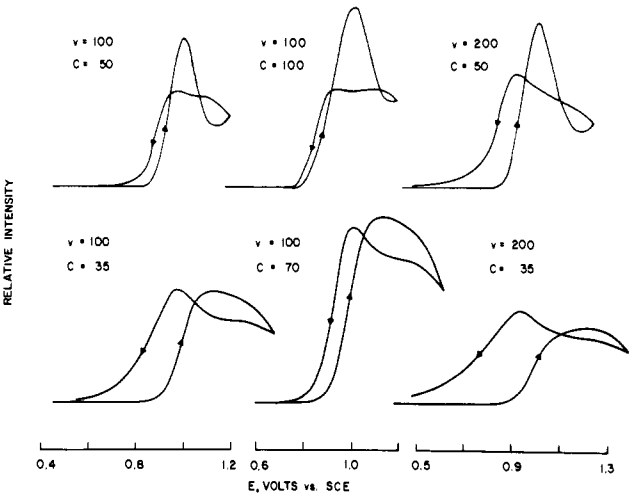


**Figure 5.** Ecl intensity–potential curves in potential scan experiments for PG/Nafion, $Ru(bpy)_3^{2+}$ in 0.2 M $Na_2SO_4$ at different scan rates ($v$ in mV/s) and with different oxalate concentrations ($C$ in mM): upper curves, experimental; lower curves, simulated. Base line is zero intensity.

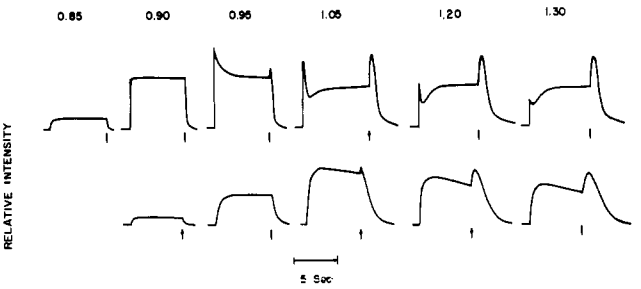


**Figure 6.** Ecl intensity–time curves in double potential step experiments for PG/Nafion, $Ru(bpy)_3^{2+}$ in 0.2 M $Na_2SO_4$ + 50 mM $Na_2C_2O_4$ (the numbers indicate the potential of the first step (V vs. SCE); the arrows indicate the time at which the potential was stepped back to 0.4 V): Upper curves, experimental; lower curves, simulated. Base line is zero intensity.

more surprising results are observed in double potential step experiments with the modified electrode. If the potential is stepped from +0.40 V, where no reaction occurs, to a more positive potential for several seconds and then back to +0.40 V, as shown in Figure 6 (upper curves), one observes an increase in the light emission intensity to an almost steady level. When the potential is stepped back to +0.40 V (or the cell is open-circuited), the light intensity first *increases* before decaying to zero. The burst of light on switching the potential to positive values and that on switching to +0.40 V are both clearly visible by eye, thus eliminating the possibility that the recorded intensity–time curves involve instrumental artifacts. The current–time curves during the same double potential step experiments do not reveal any unusual behavior; i.e., the anodic current drops immediately upon stepping back to the initial potential. Bubbling $N_2$ through the solution did not affect the ecl behavior, other than to increase the total intensity.[30]

The influence of oxalate concentration on the ecl intensity–time curves in the potential step experiments is presented in Figure 7. Clearly, increasing the oxalate concentration in the solution causes an increase in the initial peak while substantially decreasing the intensity and duration of the second peak. The effect of electrode material is shown in Figure 8. No significant change is observed for the second ecl peak while the initial peak is substantially smaller for GC and Pt compared to PG.

The qualitative behavior of the ecl intensity in potential scan or potential step experiments was perfectly reproducible, even though the exact shape of the peaks (i.e., height and width) might change from one set of experiments to another. The behavior when both $Ru(bpy)_3^{2+}$ and oxalate were dissolved in aqueous solution containing 50 mM oxalate and 1 mM $Ru(bpy)_3^{2+}$ (Figure 9) the

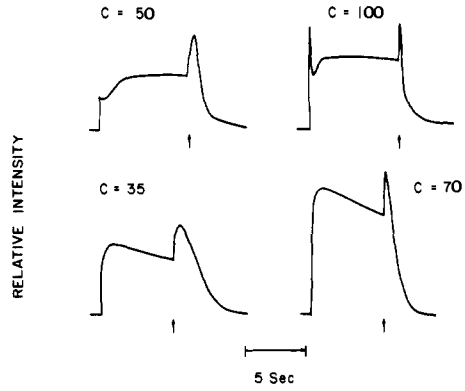


**Figure 7.** Same as Figure 6, at different oxalate concentrations ($C$ in mM). The first potential step is to 1.30 V (SCE).


**Figure 8.** Same as Figure 6, for different substrates (experimental curves). The first potential step is to 1.10 V (SCE).

ecl intensity–potential curve now features only one reverse maximum, which is not affected by the scan rate. *No* peaks are observed in the potential step experiments.

**Theoretical Model.** The sequence of reactions which occur when $Ru(bpy)_3^{2+}$ is oxidized at an electrode in the presence of oxalate ions and which produces the intense luminescence has been discussed before[30] and is presented in eq 1–7. The most striking aspect of the ecl behavior at the polymer film is the sharp increase in light intensity when the potential is returned to the initial value. Two alternative mechanisms can be envisioned that account for this unexpected observation.

**(a) The "Excited-State Production" Mechanism.** Here one assumes that reaction 4b is predominant over reaction 4a; i.e., very little or no excited state is produced by the direct reaction of $CO_2^{-\cdot}$ with $Ru(bpy)_3^{3+}$. This possibility was suggested for the reaction of thianthrene radical cation in nonaqueous solution,[42] but no independent evidence is available for the $Ru(bpy)_3^{3+}$ system.[30] In this mechanism, only a fraction of the available $CO_2^{-\cdot}$ will generate the excited state. This fraction will depend on the relative magnitudes of $k_2$ and $k_3$ and on the concentration ratio [2+]/[3+] at any instant. As the potential is stepped or scanned back (or the circuit is opened) the 3+ concentration sharply decreases, and one can expect an initial *increase* of the ecl as a larger fraction of the $CO_2^{-\cdot}$ is consumed by reaction 6 rather than (4b), before the luminescence eventually decays to zero.

**(b) The "Excited-State Quenching" Mechanism.** It is very likely that some of the $Ru(bpy)_3^{2+*}$ will be quenched by $Ru(bpy)_3^{3+}$, as shown in eq 8. This quenching is probably via an electron-

$$Ru(bpy)_3^{2+*} + Ru(bpy)_3^{3+} \xrightarrow{k_q} Ru(bpy)_3^{3+} + Ru(bpy)_3^{2+} \quad (8)$$

transfer reaction, since the reduction of $Ru(bpy)_3^{3+}$ by the excited $Ru(bpy)_3^{2+*}$ is thermodynamically favorable by more than 2 eV[42] and should be very fast. Equation 8 predicts that the oxidized form, $Ru(bpy)_3^{3+}$, while producing the ecl according to eq 2–7, will tend to reduce the ecl intensity when an excess of the 3+ form is present and it is not consumed quickly enough by the oxalate. Pulsing or scanning the potential back to values where the 3+ form is reduced (or opening the circuit so that the 3+ concentration

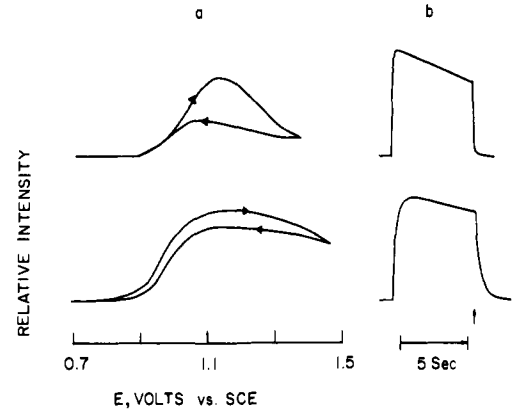


**Figure 9.** Ecl–potential at 100 mV/S (a) and ecl–time (b) curves for a PG electrode in a solution of 1.0 mM $Ru(bpy)_3(ClO_4)_2$ + 50 mM $Na_2C_2O_4$ in 0.2 M $Na_2SO_4$ (the first potential step in b is to 1.30 V (SCE)): upper curves, experimental; lower curves, simulated. Base line is zero intensity. (For details, see text.)

rapidly decreases by reaction with oxalate) would then first have the effect of removing the quencher and increasing the light intensity, before it eventually drops to zero.

Both mechanisms relate to an excess of $Ru(bpy)_3^{3+}$ available at any instant to participate either in reaction 4b or in reaction 8. Both qualitatively explain (a) the increase of the ecl reversal peak with increasing applied potential, as shown in Figure 5, since at higher potentials the excess of free $Ru(bpy)_3^{3+}$ will be greater and (b) the substantial relative decrease of the ecl reversal peak or the second reverse peak in the potential scan experiments, upon doubling the oxalate concentration, as shown in Figures 5 and 7. In the latter, an increase in the oxalate concentration reduces the free $Ru(bpy)_3^{3+}$ concentration and the quenching effect.

Another process which also contributes to the form of the ecl emission is the direct oxidation of oxalate at the electrode (substrate) surface. As already demonstrated in Figure 4, at higher positive potentials some direct oxalate oxidation has to be considered. This would also tend to reduce the ecl intensity at higher positive potentials and therefore produce a maximum when the potential is scanned back. Since the reversal ecl peak already occurs at relatively low potentials (see Figure 6), and as the simulation results described below also show, direct oxalate oxidation is responsible for the occurrence of the first reverse peak in the potential scan experiments. However, it does not contribute to the ecl peaks seen with the polymer modified electrodes in potential step experiments. As shown in Figure 9, no ecl backstepping peak occurs on a bare PG electrode with the $Ru(bpy)_3^{2+}$ dissolved in solution. This can be attributed to the substantially higher concentration of Ru species in the polymer layer (~0.5 M vs. $1 \times 10^{-3}$ M), thus creating a large excess of the 3+ species in the polymer.

The initial sharp light peak found in the potential step experiments (see Figure 6) appears to be due to an excess of oxalate ions initially adsorbed on the electrode at the electrode–polymer interface. The absence of the corresponding ecl peak with the bare PG electrode suggests that this adsorption is greatly enhanced by the polymer layer, perhaps because of the less polar environment in the polymer as compared to water. There are several indications that the initial peak is caused by an excess of oxalate adsorbed on the electrode surface. (a) As shown in Figure 6, the initial ecl peak is absent for steps to less positive potentials, where the concentration of electrogenerated 3+ Ru species is small and the ecl reaction is not limited by the oxalate concentration. (b) The peak appears at more positive potentials and then gradually decreases at high applied potentials, where the adsorbed oxalate can be directly oxidized at the electrode. (c) The initial peak increases with increasing oxalate concentration, as shown in Figure 7; this can be attributed to a larger amount of adsorbed oxalate, assuming that the substrate surface is not saturated. (d) The initial peak is substantially smaller with modified Pt and GC than with PG, as shown in Figure 8. This may be caused by the much larger

(42) Chang, M.-M.; Saji, T.; Bard, A. J. *J. Am. Chem. Soc.* **1977**, *99*, 5399.
(43) Sutin, N. *J. Photochem.* **1979**, *10*, 19.

actual surface area of the PG as compared to Pt or GC, resulting in a higher amount of adsorbed oxalate, while the ecl reaction is, to a large degree, limited by diffusion of the Ru species, which is related to the geometric area of the substrate.

**Digital Simulation.** The validity of the model and the different mechanisms suggested was tested by examining if the ecl behavior can be qualitatively reproduced by digital simulation. The principles of digital simulation techniques for electrochemical systems under partial diffusion control have been discussed previously[15,40,44] and will not be given here. We will discuss, however, the special considerations and complications involved in the simulation of the present system.

Generally, the computer simulation program included the following steps: charge transfer at the substrate/polymer interface for Ru species with some direct oxalate oxidation, both processes being potential dependent; diffusion of the various species in the polymer layer, according to Fick's laws; the reaction between $Ru(bpy)_3^{3+}$ and oxalate, according to eq 2; generation of the excited state (eq 3–4a, 6–7, with the possibility of replacing eq 4a with eq 4b, to test the "excited-state production" mechanism), which either luminesces (eq 5a) or is possibly quenched (eq 8); and calculation of both the current and the ecl in each time element. We discuss in the following paragraphs the specific way in which these processes are accounted for in the program. (1) The experimental electrochemical results yielded a diffusion coefficient for the Ru species in the polymer of the order of $10^{-9}$ $cm^2/s$. This small value results in a diffusion layer, even in cyclic voltammetry (CV) experiments, which extends only ~10% of the polymer layer thickness. Thus, the polymer layer can be taken as a bulk source of Ru species, which move to or from the electrode under diffusion control. (2) For the electron-transfer reaction of the $Ru(bpy)_3^{3+/2+}$ at the electrode (eq 1), we assumed a simple one-electron single-step reaction, with $\alpha = 0.5$. The heterogeneous rate constant, $k^\circ$, was found from the experimental CV results, by simulating the CV curve of PG/Nafion, $Ru(bpy)_3^{2+}$ (Figure 2a), as shown below. (3) For the direct overall oxalate oxidation on the electrode, as given in eq 9, we assumed an irreversible

$$C_2O_4^{2-} \rightarrow 2CO_2 + 2e^- \quad (9)$$

reaction with the first electron-transfer rate determining. The values of $k^\circ$(oxalate), $E^\circ$(oxalate), $C^*_{oxal}$(oxalate concentration in the polymer), and D (oxalate) (diffusion coefficient of oxalate in the polymer) were derived by simulating curves 2b and 4b, as discussed below. (4) Reaction 2 was taken to be first order with respect to both reactants, and the rate constant $k_1$ was derived by fitting curve 2b. The main difficulty, however, in simulating this step is the large difference between the diffusion coefficients of Ru species and oxalate in the polymer, as discussed above, which means that the diffusion layer of the oxalate is much larger than that of the Ru species. In terms of the simulation, if one wishes to treat the reaction between the $Ru(bpy)_3^{3+}$ and $C_2O_4^{2-}$, one has to use a very large number of space elements of the size needed for the Ru species to account for $C_2O_4^{2-}$ diffusion, which is not practical. We chose to solve this problem by assuming that the whole diffusion layer for the Ru species is included in the first "oxalate-box" adjacent to the electrode, an assumption which is justified by the relative size of the diffusion coefficients. This means, therefore, that the oxalate concentration is uniform in all of the Ru boxes, which also simplified the calculations. The diffusion of the Ru species and the oxalate ions were then calculated separately. (5) The "excited-state production" mechanism was taken into account in the following manner: reaction 7 is probably very fast (diffusion controlled); i.e., all 1+ species generated in reaction 6 will rapidly produce the excited state. Under these conditions and if one also assumes that during each time element the concentrations of 2+ and 3+ Ru species are approximately constant, the $Ru(bpy)_3^{2+*}$ produced in each element will be given by eq 10, assuming, in this case, that reaction 4 is negligible. (6) For the quenching mechanism, the size of the time

$$[2+^*] \propto [CO_2^{-}\cdot] \frac{k_2[2+]}{k_2[2+] + k_3[3+]} \quad (10)$$

elements in the program, which is chosen to be small enough to simulate the diffusion processes, is much too long to account for the short lifetime of the excited state (0.6 μs[45,46]) and the fast quenching kinetics (eq 8). We used, therefore, the method suggested by Feldberg[47,48] and Faulkner and co-workers,[49,50] where the diffusion, the electron-transfer processes, and the excited-state production are simulated in the usual manner, while in each time element the ecl intensity is calculated by analytically solving the kinetic equations. In the present case, the ecl intensity was calculated in each time interval as

$$-\frac{d[2+^*]}{dt} = k_4[2+^*] + k_q[2+^*][3+] \quad (11)$$

($Ru(bpy)_3^{2+*}$ and $Ru(bpy)_3^{3+}$ are denoted 2+* and 3+, respectively) where $k_4$ is the combined rate constant for the radiative and nonradiative decay and $k_q$ is the rate constant for the quenching process, eq 8. The concentration of the excited state is then given by eq 12, where $[2+^*]^\circ$ is the initial concentration

$$[2+^*] = [2+^*]^\circ \exp(-kt) \quad (12)$$

of excited state, which is in fact the concentration of $CO_2^{-}\cdot$ formed; and k is given by eq 13. The rate of light emission is given by

$$k = k_4 + k_q[3+] \quad (13)$$

$k_r[2+^*]$, where $k_r$ is the rate constant for the radiative decay; thus the relative ecl intensity, $I$, in each time interval $\Delta t$ can be calculated by eq 14. The value of $k_r$ is $1.7 \times 10^6$ $s^{-1}$,[45,46] and $k_4$

$$I \propto \int_0^{\Delta t} [2+^*]\, dt = [2+^*]^\circ k^{-1}[1 - \exp(-k\,\Delta t)] \quad (14)$$

was estimated to be 1 order-of-magnitude larger.[51] (7) The experimental results suggested that the first ecl peak in the potential step experiments is caused by an excess of oxalate initially adsorbed on the electrode. Inclusion of this phenomenon in the simulation program is not straightforward and indeed would involve complicated modifications, since we assumed that the first "oxalate box", which would be the one to accommodate the excess oxalate ions, is in fact larger than the whole diffusion layer of the Ru species. We, therefore, did not attempt to treat this initial ecl peak found with PG in the simulation.

**Digital Simulation Results.** The points in Figure 2a represent the simulated current–potential curve for a PG/Nafion, $Ru(bpy)_3^{2+}$ electrode in background solution. The simulation parameters were [2+] = 0.5 M, $D(2+) = 1.0 \times 10^{-9}$ $cm^2/s$, and $k^\circ(2+/3+) = 2.4 \times 10^{-5}$ cm/s. The source of the *apparent* small value of the heterogeneous rate constant $k^\circ$ which accounts for the large $\Delta E_p$, compared to the value for dissolved Ru species, is currently being investigated. Figure 2b is a representation of the experimental and simulated current–potential simulation parameters where $D(3+) = 0.5 \times 10^{-9}$ $cm^2/s$, $[C_2O_4^{2-}] = 35$ mM, $D(C_2O_4^{2-}) = 8.0 \times 10^{-7}$ $cm^2/s$, $k_1 = 30$ $M^{-1}$ $s^{-1}$; $k^\circ$(oxalate) = $1.0 \times 10^{-10}$ cm/s, and $E^\circ$(oxalate) = 0.55 V; the other parameters had the same values as those in Figure 2a.

There are several points to be noted here. (a) The values taken for $[C_2O_4^{2-}]$ and $D(C_2O_4^{2-})$ appear reasonable, in view of the apparently relatively free movement of $C_2O_4^{2-}$ ions in the film, as discussed previously. (b) The exact values of $k^\circ$(oxalate) and $E^\circ$(oxalate) pertaining to the direct oxalate oxidation on the electrode or the detailed mechanism for this step are not crucial in simulating the results; this reaction was added mainly to examine the contribution of some direct oxalate oxidation at high

(44) Feldberg, S. W. In "Electroanalytical Chemistry"; Bard, A. J., Ed.; Marcel Dekker: New York, 1969; Vol. 3.
(45) Navon, G.; Sutin, N. *Inorg. Chem.* **1974**, *13*, 2159.
(46) Demos, J. N.; Addington, J. W. *J. Am. Chem. Soc.* **1976**, *15*, 5800.
(47) Feldberg, S. W. *J. Phys. Chem.* **1966**, *70*, 3928.
(48) Feldberg, S. W. *J. Am. Chem. Soc.* **1966**, *88*, 390.
(49) Bezman, R.; Faulkner, L. R. *J. Am. Chem. Soc.* **1972**, *94*, 3699.
(50) Morris, J. L.; Faulkner, L. R. *J. Electrochem. Soc.* **1978**, *125*, 1079.
(51) Wallace, W. L.; Bard, A. J. *J. Phys. Chem.* **1979**, *83*, 1350.

positive potentials to the shape of the ecl curves. The value of 0.55 V for $E^\circ$(oxalate), far more positive than the thermodynamic redox potential for oxalic acid,[52] is, however, a reasonable estimation for the first electron transfer.[30] (c) We attempted to measure $k_1$ independently by studying the catalytic oxidation of $C_2O_4^{2-}$ in solution by $Ru(bpy)_3^{3+}$ electrogenerated at a GC electrode by cyclic voltammetry. Although this measurement is complicated by the contribution from the direct oxidation of oxalate on the GC, we estimate a rate constant of $\sim 10^4$ $M^{-1}$ $s^{-1}$ (in solution). However, the electrochemical and ecl data for the polymer-coated electrodes cannot be fitted with $k_1$ values which are this high. The best fit was obtained with $k_1 = 30$ $M^{-1}$ $s^{-1}$, which suggests that the reaction between attached $Ru(bpy)_3^{3+}$ and oxalate in the polymer is much slower than the same reaction in solution.

For simulation of the ecl behavior, the program was constructed in a manner that allows inclusion of either the "excited-state production" mechanism, the quenching mechanism, or both. As expected, both mechanisms qualitatively reproduce the basic ecl behavior, namely, the back-scanning and back-stepping peaks. If one considers *quenching only*, reverse ecl peaks can be simulated, with $k_q \approx 2 \times 10^9$ $M^{-1}$ $s^{-1}$. However, the simulated peaks are significantly broader than experimentally observed, which suggests that quenching *alone* does not account for the observed peaks.

A better simulated behavior of PG/Nafion, $Ru(bpy)_3^{2+}$ electrode in aqueous oxalate solution is achieved if one also considers the "excited-state production" mechanism, as presented in Figures 5–7. All the simulation parameters are the same as in Figure 2b; the "excited-state production" mechanism is included, with $k_3/k_2 = 2$; and some quenching of the excited state by the 3+ species is also included, with $k_q = 5 \times 10^7$ $M^{-1}$ $s^{-1}$. It is satisfying that in this manner the semiquantitative behavior of the ecl curves, primarily the various peaks observed on scan or step reversal, are reproduced by the simulation program (excluding the initial peak in the potential step experiments, as discussed before). One difference between the experimental and simulated ecl curves is that in the simulation the quasi-steady-state luminescence in the potential steps tends to decrease more rapidly in the simulated results than it does experimentally. This difference is probably due to the approximations used in the program and possibly also to the fact that side reactions, e.g., the reaction of $CO_2^{-\cdot}$ and $Ru(bpy)_3^{+}$ with water, were not included. The model predicts the appearance of the different luminescence peaks, and the effect of changing the oxalate concentration or scan rate. As shown in Figure 9, the program can also be used to simulate bare electrode-dissolved $Ru(bpy)_3^{2+}$ conditions. If we take the values [2+] = 1.0 mM, $[C_2O_4^{2-}] = 50$ mM, $k^\circ(3+/2+) = 0.07$ cm/s,[38] $D(2+) = 6.1 \times 10^{-6}$ $cm^2/s$,[38] $D(3+) = 5.2 \times 10^{-6}$ $cm^2/s$,[38] $D$(oxalate) $= 2 \times 10^{-5}$ $cm^2/s$, and $k_1 = 1 \times 10^4$ $M^{-1}$ $s^{-1}$, with the other parameters the same as for the modified electrode, the simulation predicts no peaks on the reverse steps, in agreement with the experimental results. By eliminating the direct electrooxidation of oxalate from the program, one can show that this process is responsible only for the first reverse ecl peak in the potential scan experiments, while the other peaks, including the large reverse potential step peak, are caused by the processes in eq 4b and 8.

Note that almost identical ecl curves are produced by the simulation program for the polymer-coated electrode if one eliminates quenching completely but uses a ratio of $k_3/k_2 = 5$ (instead of 2, with quenching). Thus, the actual contribution of each of the two paths to the observed ecl behavior cannot be established from the ecl and electrochemical results alone. Independent measurements of the rate constants and evaluation of the contribution of quenching are required before a more definite mechanism can be proposed.

(52) Latimer, W. M. "Oxidation Potentials", 2nd ed.; Prentice Hall: 1956; p 131.

## Conclusions

Electrodes coated with a Nafion film in which large amounts of electroactive materials are incorporated were shown to be very stable in aqueous solution, with possible catalytic properties. The apparent diffusion coefficient of the attached Ru complex is $\sim 10^{-9}$ $cm^2/s$, which makes the catalytic process for these thick coatings crucially dependent on the ease of penetration of the substrate molecules into the polymer layer. Oxalate ions easily penetrate into the Nafion layer, and the mediated oxidation, which subsequently causes the production of luminescence, is, therefore, efficient. Combining ecl data with the usual electrochemical results creates a powerful tool for studying the nature of the reactions occurring at modified electrodes and, in our case, we were able to propose a model which accounts for essentially all of the experimental results. The model included mediated oxidation of oxalate by $Ru(bpy)_3^{3+}$ formed upon oxidation of $Ru(bpy)_3^{2+}$ at the substrate surface, as well as direct oxalate oxidation on the substrate. It also demonstrated the possibility that only a fraction of the ecl is produced by direct reaction of $CO_2^{-\cdot}$ with $Ru(bpy)_3^{3+}$ and that quenching of the emitting $Ru(bpy)_3^{2+*}$ by an excess of $Ru(bpy)_3^{3+}$ is also possible. Estimates for the rate constants of the various processes were obtained by digital simulation of the current–potential and ecl curves. The simulated curves were in good semiquantitative agreement with the experimental results. In addition to the usefulness of these electrodes in elucidating transport and electron-transfer processes in polymer films, several applications are possible. These include electrochemical analysis of trace components by concentration into the film, as previously suggested by Oyama and Anson[3] for polyvinylpyridine-coated electrodes and the electrocatalysis of slow reactions (e.g., mediation of enzyme redox processes). Electrochemical display devices, either active (ecl) or passive (electrochromic, e.g., involving polymer-bound $MV^{2+}$ or other species), also appear possible.

**Acknowledgment.** The support of this research by the Army Research Office (Grant DAAG 29-78-G-0191) is gratefully acknowledged. We are also indebted to Professor Fred Anson and Mr. D. Buttry for helpful discussions and suggestions concerning the reaction mechanism.